PNAS RESEARCH ARTICLE | IMMUNOLOGY AND INFLAMMATION

Both intratumoral regulatory T cell depletion and CTLA-4 antagonism are required for maximum efficacy of anti-CTLA-4 antibodies

Brianna M. Lax[a,b], Joseph R. Palmeri[a,b], Emi A. Lutz[a,c], Allison Sheen[a,c], Jordan A. Stinson[a,c], Lauren Duhamel[a,c], Luciano Santollani[a,b], Alan Kennedy[d], Adrienne M. Rothschilds[a,c], Stefani Spranger[a,e], David M. Sansom[d], and K. Dane Wittrup[a,b,c,1]

Edited by Alexander Rudensky, Memorial Sloan Kettering Cancer Center, New York, NY; received January 16, 2023; accepted June 23, 2023

Anti-CTLA-4 antibodies have successfully elicited durable tumor regression in the clinic; however, long-term benefit is limited to a subset of patients for select cancer indications. The incomplete understanding of their mechanism of action has hindered efforts at improvement, with conflicting hypotheses proposing either antagonism of the CTLA-4:B7 axis or Fc effector-mediated regulatory T cell (Treg) depletion governing efficacy. Here, we report the engineering of a nonantagonistic CTLA-4 binding domain (b1s1e2) that depletes intratumoral Tregs as an Fc fusion. Comparison of b1s1e2-Fc to 9d9, an antagonistic anti-CTLA-4 antibody, allowed for interrogation of the separate contributions of CTLA-4 antagonism and Treg depletion to efficacy. Despite equivalent levels of intratumoral Treg depletion, 9d9 achieved more long-term cures than b1s1e2-Fc in MC38 tumors, demonstrating that CTLA-4 antagonism provided additional survival benefit. Consistent with prior reports that CTLA-4 antagonism enhances priming, treatment with 9d9, but not b1s1e2-Fc, increased the percentage of activated T cells in the tumor-draining lymph node (tdLN). Treg depletion with either construct was restricted to the tumor due to insufficient surface CTLA-4 expression on Tregs in other compartments. Through intratumoral administration of diphtheria toxin in Foxp3-DTR mice, we show that depletion of both intratumoral and nodal Tregs provided even greater survival benefit than 9d9, consistent with Treg-driven restraint of priming in the tdLN. Our data demonstrate that anti-CTLA-4 therapies require both CTLA-4 antagonism and intratumoral Treg depletion for maximum efficacy—but that potential future therapies also capable of depleting nodal Tregs could show efficacy in the absence of CTLA-4 antagonism.

immunotherapy | CTLA-4 | Tregs | cancer | protein engineering

Significance

Anti-CTLA-4 antibodies have revolutionized cancer treatment, but their mechanism of action is not well understood. Previous attempts to elucidate their mechanism have lacked a construct capable of intratumoral Treg depletion without CTLA-4 antagonism. We compared the administration of a nonantagonistic CTLA-4 binder (b1s1e2-Fc) and an antagonistic anti-CTLA-4 antibody (9d9) in a syngeneic mouse tumor model. Both constructs equivalently depleted Tregs, but only mice treated with 9d9 showed signs of enhanced T cell activation. 9d9 provided greater survival benefit than b1s1e2-Fc, demonstrating the necessity of both functions for maximum antitumor efficacy. CTLA-4-agnostic depletion of both intratumoral and nodal Tregs achieved even greater antitumor efficacy, suggesting that targeting nodal Tregs could be a promising strategy for enhancing the potency of existing immunotherapies.

Cytotoxic T-lymphocyte-associated protein-4 (CTLA-4) is an inhibitory receptor expressed constitutively at high levels on Foxp3$^+$ regulatory T cells (Tregs) and transiently at lower levels on conventional T cells upon activation (1, 2). CTLA-4 and its costimulatory homologue, CD28, share the endogenous ligands B7.1 (CD80) and B7.2 (CD86), allowing for modulation of immune responses. CTLA-4 has a significantly higher affinity for both B7.1 and B7.2 than CD28 does, allowing CTLA-4 to outcompete CD28 for binding to B7 and physically exclude CD28 from immunological synapses (3–5). Lack of CD28:B7 binding deprives T cells of this essential costimulatory signal, resulting in improper activation and a dysfunctional phenotype. Tregs further suppress immune activation by reducing B7 levels on antigen-presenting cells (APCs) via transendocytosis, a cell-extrinsic function in which CTLA-4 physically removes B7 from APC cell membranes, internalizes, and directs the ligand for lysosomal degradation (6, 7).

Tregs are essential for the maintenance of immune homeostasis, requiring the forkhead transcription factor Foxp3 for development and CTLA-4 expression for immunosuppressive functionalities (8–12). As a result, both CTLA-4$^{-/-}$ and Foxp3$^{-/-}$ mice die at a very young age from severe lymphoproliferative disease (9, 13, 14). Despite the importance of systemic Tregs, increased Treg infiltration in the tumor microenvironment (TME) is correlated with poor prognosis in patients for various cancer indications (15–18). Intratumoral Tregs contribute to the immunosuppressive cytokine pool in the TME, most commonly producing interleukin-10 (IL-10), IL-35, and transforming growth factor-beta (TGF-β) (19–21). These cytokines, along with other immunosuppressive factors, limit the activation and function of cytotoxic T cells and promote in situ induction of additional Tregs (22–25). Tregs also restrain the induction of antitumor immune responses in tdLNs, and since effector T cells and Tregs are primed via the same canonical mechanisms, the tdLN acts as a source of both effector T cells and Tregs (26–30). While some Tregs traffic to the tumor, others accumulate in the tdLN throughout tumor progression, dampening T cell

The authors declare no competing interest.

This article is a PNAS Direct Submission.

[1]To whom correspondence may be addressed. Email: wittrup@mit.edu.

This article contains supporting information online at https://www.pnas.org/lookup/suppl/doi:10.1073/pnas.2300895120/-/DCSupplemental.

Published July 24, 2023.

priming, producing anti-inflammatory cytokines, generating immune tolerance against cancer antigens, and even directly killing dendritic cells (31–35). The development of Foxp3-DTR mouse models, where diphtheria toxin receptor (DTR) expression is linked to Foxp3 expression, has allowed for selective Treg depletion via diphtheria toxin (DT) administration (36–38). These models have been used to highlight the antitumor potential of Treg depletion, demonstrating that depleting 90% of intratumoral Tregs results in impressive cure rates (39, 40). However, the associated systemic Treg depletion results in severe, and often fatal, autoimmunity (41).

Anti-CTLA-4 antibodies were developed to improve endogenous antitumor responses via "releasing of the brakes" on T cells. Ipilimumab became the first checkpoint blockade immunotherapy to be FDA approved based on a phase III clinical trial in patients with metastatic melanoma (42). Since then, ipilimumab has been approved for several other cancer indications, and most recently, tremelimumab was approved in combination with durvalumab (anti-PD-L1) (43). Despite this clinical success, the mechanism of anti-CTLA-4 antibodies is still debated (44–53). Anti-CTLA-4 antibodies were originally hypothesized to function by antagonizing CTLA-4, leading to enhanced priming in tdLNs through increased engagement of CD28 with B7 (54). Many reports use anti-CTLA-4 antibodies in combination with other agents to boost priming of effector T cells and improve antitumor immune responses (55–60). However, the interaction of anti-CTLA-4 antibodies with Tregs became a topic of interest after the discovery of Treg proliferation in the tdLN following treatment (61, 62). Evidence supporting intratumoral Treg depletion via antibody-dependent cellular cytotoxicity/phagocytosis (ADCC/P) identified another possible mechanism of action (63–68). The importance of Treg depletion for anti-CTLA-4 therapeutic efficacy in mouse models has been shown through the use of effector-dead Fcs or $Fc\gamma R^{-/-}$ mice, both of which abrogate efficacy (69). Most recently, a third hypothesis for how anti-CTLA-4 antibodies function argues that the majority of efficacy is a result of myeloid compartment reprogramming via FcγR interactions (52, 53). While these studies demonstrated that neither CTLA-4 antagonism nor intratumoral Treg depletion was efficacious in the absence of FcγR interactions, all tested FcγR-engaging constructs also antagonized CTLA-4, confounding the effects of these two functions. In an attempt to remove the antagonistic function from anti-CTLA-4 therapies, a weakly antagonistic antibody that retains Treg-depleting capabilities was reported that performed at least as well as ipilimumab in transgenic mice expressing human CTLA-4 (70). While this antibody does not have full antagonistic effects in vitro, mice with human CTLA-4 and murine B7 do not recapitulate the endogenous interactions of the CTLA-4:B7 axis in wild-type mice.

To explore the individual contributions of antagonism and Treg depletion to anti-CTLA-4 therapeutic efficacy, we developed an anti-CTLA-4 antibody-like construct whose epitope is distinct from that of B7.1. This construct allowed us to test CTLA-4-mediated Treg depletion in the absence of antagonism. We compared the therapeutic efficacy of this construct to an antagonistic antibody, each with both an activating and an effector-dead murine Fc (mIgG2c). Using this panel of four constructs, each with the ability to antagonize CTLA-4, deplete intratumoral Tregs, do neither, or do both, we were able to directly assess efficacy contributed by each function. We found that CTLA-4 antagonism and Treg depletion are synergistic—the construct with both functions achieved the highest cure rate. Consistent with previous reports, we found that while CTLA-4 antagonism enhanced $CD8^+$ and $CD4^+$ T cell activation in the tdLN, this also included Tregs. The lack of nodal Treg depletion can be attributed to insufficient surface CTLA-4 expression to elicit ADCC/P. Through intratumoral (i.t.) administration of DT to Foxp3-DTR mice, we depleted both intratumoral and nodal Tregs, resulting in superior tumor control compared to that of anti-CTLA-4 antibodies. This demonstrates that future therapies could provide enhanced antitumor efficacy through the ability to selectively deplete both intratumoral and nodal Tregs.

Results

Development of B7-Noncompetitive CTLA-4 Binders. We identified B7-noncompetitive CTLA-4 binders using yeast surface display (YSD) with two previously developed libraries: a synthetic, human single-chain variable fragment (scFv) library and a charge-neutralized Sso7d scaffold library (71, 72). The Sso7d scaffold was generated from a small DNA-binding protein and has previously been used to make murine therapeutic binders (73). These CTLA-4 binders were selected for as previously described using a soluble form of murine CTLA-4 fused to the CH2-CH3 domains of the mIgG2c Fc (CTLA-4-Fc) (3, 74). Several rounds of flow-assisted cell sorting (FACS) were performed to enrich for binders with the highest affinity to CTLA-4-Fc. To bias selections for binders with a unique epitope, we performed our sorts in the presence of excess soluble B7.1-Fc to mask its epitope on CTLA-4.

The Sso7d library converged on a single clone (b1s1) with modest affinity to CTLA-4-Fc when b1s1 was displayed on the surface of yeast and undetectable affinity to cell surface CTLA-4 when b1s1 was purified as a soluble, monomeric protein. Two rounds of affinity maturation were performed, introducing four framework mutations (Fig. 1 *A* and *B*). While one-log fold improvement in affinity was achieved through the first round (b1s1e1), a second round was unable to further improve the affinity on the surface of yeast (b1s1e2) (Fig. 1*C*). We hypothesized that the lack of further improvement in affinity was related to the avidity afforded by the yeast display system. To circumvent the lack of avidity in the soluble, monomeric format and mimic the mIgG2c antibody format of 9d9 for dosing in vivo, we created b1s1e2-Fc via fusion of the Sso7d to the CH2-CH3 domains of the mIgG2c Fc separated by a flexible linker (Fig. 1*D*). Although there was still a reduction in affinity compared to the yeast displayed format, b1s1e2-Fc and 9d9 had equivalent affinities to cell surface CTLA-4, enabling direct comparison of the two therapies (Fig. 1*E*). Attempts to identify an antibody scFv fragment were discontinued due to lack of in vivo Treg depletion (*SI Appendix*, Fig. S1 *A–E*).

b1s1e2-Fc Binding Does Not Block the CTLA-4:B7 Axis. We developed a CTLA-4 YSD system to confirm that b1s1e2-Fc has a distinct epitope from B7.1. Mutant libraries of CTLA-4 displayed on the surface of yeast were generated, and several rounds of FACS were performed to enrich for nonbinders to either B7.1-Fc or b1s1e2-Fc (*SI Appendix*, Fig. S2 *A* and *B*) (75). Epitope mapping of B7.1 was used to validate this system, and the identified residues were consistent with the reported B7.1 epitope (*SI Appendix*, Table S1) (76, 77). The b1s1e2-Fc epitope mapping revealed a single residue required for binding, F67, located in a loop positioned orthogonally to the B7.1 epitope, confirming that these epitopes are completely distinct (Fig. 1*F* and *SI Appendix*, Table S2). To confirm these results, either $CTLA\text{-}4^{WT}$ or $CTLA\text{-}4^{F67L}$ was expressed on the surface of HEK293-F cells. While 9d9 binding was equivalent to both $CTLA\text{-}4^{WT}$ and $CTLA\text{-}4^{F67L}$, b1s1e2-Fc binding was completely abrogated to $CTLA\text{-}4^{F67L}$ (Fig. 1*G*). Epitope mapping of the discontinued antibody revealed

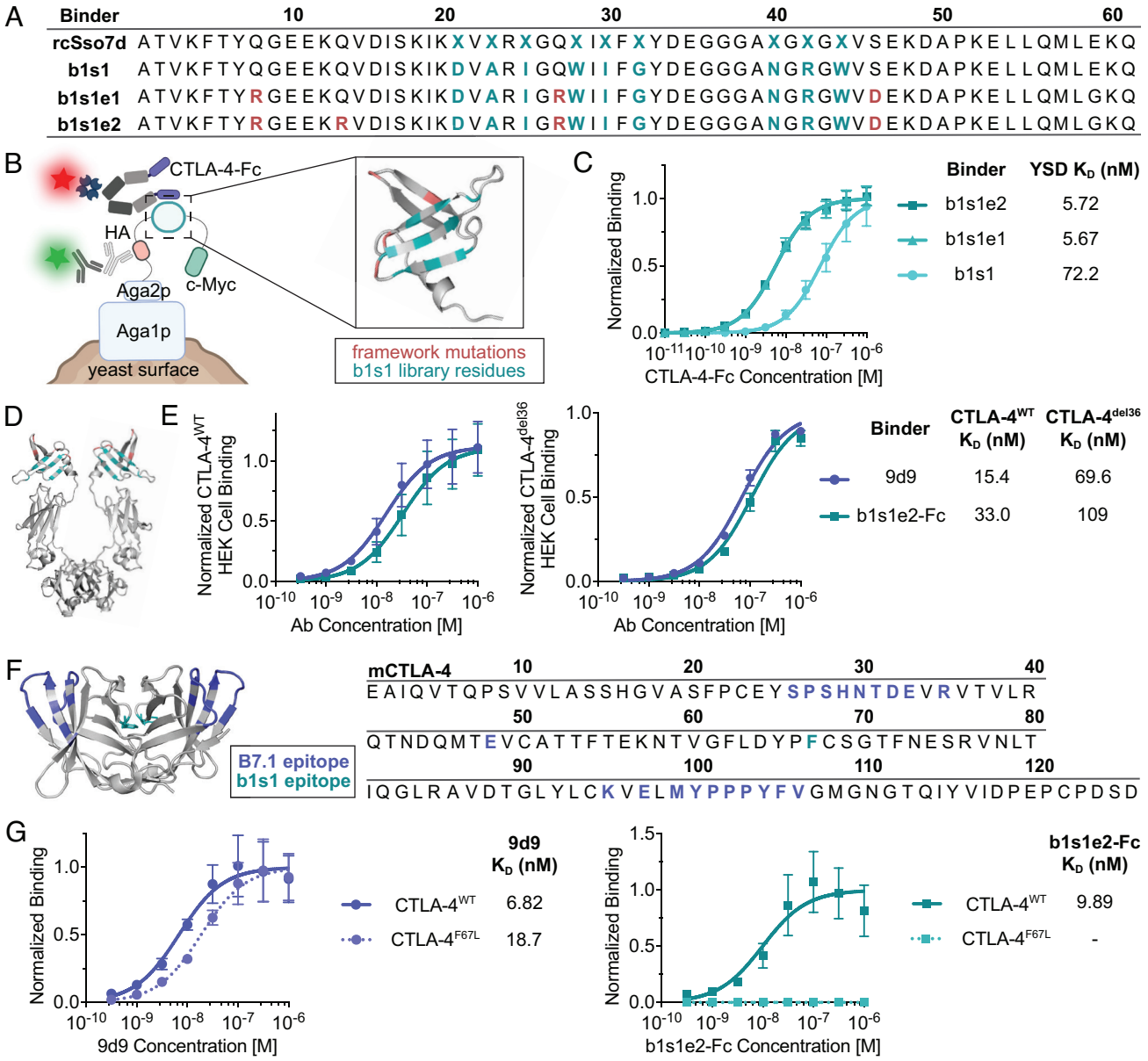

Fig. 1. Development of B7-noncompetitive CTLA-4 binders. (*A*) Amino acid sequences of Sso7d CTLA-4 binders. The residues of b1s1 at the nine randomly mutated sites in the rcSso7d-11 library are shown in teal; framework mutations introduced during affinity maturation are shown in coral. (*B*) Schematic of the yeast surface display (YSD) system used for identification and affinity maturation of CTLA-4 binders using the Sso7d scaffold. Sso7d binder display was detected using a fluorescent antibody against the hemagglutinin (HA) tag (AF488, green), and binding to soluble biotinylated CTLA-4-Fc was detected using a fluorescent streptavidin conjugate (SA-AF647, red). The protein structure of b1s1e2 is shown with highlighted mutations (PDB ID: 1SSO). (*C*) Equilibrium binding curves of Sso7d binders transformed as single clones into yeast. Binding affinities (K_D values, equilibrium dissociation constants) to soluble, biotinylated CTLA-4-Fc were calculated using a nonlinear regression fit for one-site total binding with no nonspecificity. Binding was measured by mean fluorescence intensity (MFI) of SA-AF647 by flow cytometry and normalized to the B_{max} values (mean ± SD; $n = 3$). (*D*) Protein structure of the engineered antibody-like construct (b1s1e2-Fc). The Sso7d binder is fused to the N terminus of the mIgG2c CH2-CH3 domains with a $(G_4S)_3$ linker (PDB ID: 6BHQ). (*E*) Equilibrium binding curves of 9d9-AF647 (purple) and b1s1e2-Fc-AF647 (teal) to a HEK293-F line stably expressing surface CTLA-4^{WT} (*E*, *Left*) (mean ± SD; $n = 4$) and CTLA-4^{del36} (*E*, *Right*) (mean ± SD; $n = 5$). Binding was measured by AF647 MFI by flow cytometry and normalized to the B_{max} values. (*F*) Protein structure (*F*, *Left*) and amino acid sequence (*F*, *Right*) of the extracellular domain of murine CTLA-4 homodimer (PDB ID: 1DQT). The B7.1 epitope is shown in purple, and the b1s1e2 epitope is shown in teal. (*G*) Equilibrium binding curves of 9d9-AF647 (*G*, *Left*) and b1s1e2-Fc-AF647 (*G*, *Right*) to transiently transfected HEK293-F cells expressing either CTLA-4^{WT} (solid lines) or CTLA-4^{F67L} (dashed lines) (mean ± SD; $n = 3$). Binding was measured by AF647 MFI by flow cytometry and normalized to the B_{max} values.

epitope inaccessibility as a potential explanation for lack of in vivo Treg depletion (*SI Appendix*, Fig. S2 *C* and *D* and Table S3) (78).

Due to the small size of the CTLA-4 extracellular domain, a distinct epitope may not be sufficient to be fully B7-noncompetitive if steric hindrance prevents simultaneous binding of b1s1e2-Fc and B7. We performed an enzyme-linked immunosorbent assay (ELISA) to quantify the reduction in binding affinity to CTLA-4 bound to a B7.1-coated plate as compared to binding directly to a CTLA-4-coated plate (Fig. 2*A*). The ability of b1s1e2-Fc to bind CTLA-4 was not affected by the binding of CTLA-4 to B7.1 but 9d9 binding was reduced by almost two-log fold (Fig. 2*B*). We also performed an ELISA to calculate the half-maximal inhibitory concentration (IC_{50}) of each binder required to inhibit B7.1 binding to CTLA-4. While increasing concentrations of b1s1e2-Fc or an irrelevant antibody (anti-CD25) had no effect on B7.1 binding, both 9d9 and unlabeled B7.1 significantly decreased B7.1 binding, with IC_{50} values of 23.5 nM and 1.72 nM, respectively (Fig. 2*C*). To confirm the lack of competition between b1s1e2-Fc and B7.1-Fc held for surface CTLA-4, we used cells expressing non-internalizing CTLA-4^{del36} (6). Similarly to the ELISA, 9d9 blocked

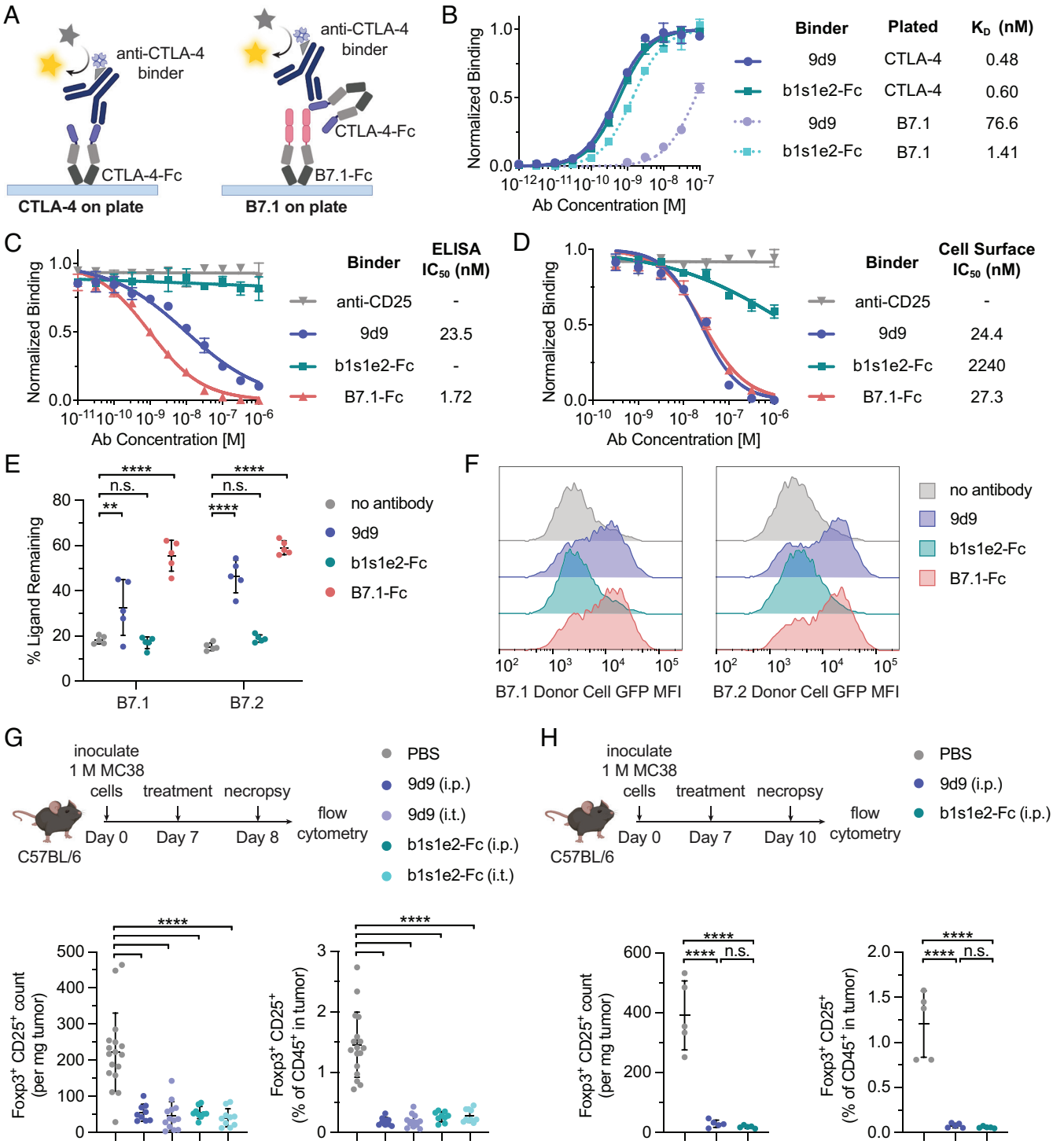

Fig. 2. Characterization of b1s1e2-Fc as a nonantagonistic, intratumoral Treg-depleting construct. (*A*) ELISAs to detect direct binding affinity to a CTLA-4-Fc-coated plate (*A*, *Left*) and indirect binding affinity to CTLA-4-Fc bound to a B7.1-Fc-coated plate (*A*, *Right*). (*B*) Equilibrium binding curves of 9d9-biotin and b1s1e2-Fc-biotin to CTLA-4-Fc on the plate (solid lines) or to CTLA-4-Fc bound to B7.1-Fc on the plate (dashed lines) (mean ± SD; $n = 3$). Binding was detected by streptavidin-horseradish peroxidase (SA-HRP), measured by 450 nm absorbance, and normalized to the B_{max} values. (*C*) Competitive ELISA detecting blocking of B7.1-Fc-biotin binding to CTLA-4-Fc with titrations of CTLA-4 binders. Inhibitory dose-response curves and the half-maximal inhibitory concentrations (IC_{50} values) were calculated assuming a one-site, reversible competition model (mean ± SD; $n = 3$). Binding was detected by SA-HRP, measured by 450 nm absorbance, and normalized. (*D*) Competitive assay detecting blocking of B7.1-Fc binding to a HEK293-F cell stable line expressing surface CTLA-4^{del36}. Inhibitory dose-response curves and IC_{50} values were calculated assuming a one-site, reversible competition model (mean ± SD; $n = 3$). Binding was measured by AF647 MFI by flow cytometry and normalized. (*E*) Transendocytosis assay detecting the ability of CTLA-4 binders to inhibit transendocytosis of B7.1 and B7.2. CHO cells expressing either B7.1-GFP or B7.2-GFP and CHO cells expressing CTLA-4 were incubated overnight at a ratio of 3:1. The amount of B7 remaining on donor cells was quantified via GFP MFI by flow cytometry and compared to that of donor cells incubated with CTLA-4^- control cells (mean ± SD; $n = 5$). (*F*) Representative histograms of GFP MFI for B7.1-expressing cells (*F*, *Left*) and B7.2-expressing cells (*F*, *Right*) (gated on single cell/live/GFP^+). (*G*) MC38-bearing mice were treated either i.p. or i.t. on day 7 with PBS, 200 μg of 9d9 WT, or 88.8 μg of b1s1e2-Fc WT (molar equivalent). Twenty-four hours later, tumors were excised and analyzed via flow cytometry for count and percentage of $Foxp3^+$ $CD25^+$ Tregs (gated on single cell/live/$CD45^+$/$CD3^+$/$CD4^+$) (mean ± SD; $n = 9$-17, data combined from five different experiments). (*H*) MC38-bearing mice were treated i.p. on day 7 with PBS, 200 μg of 9d9 WT, or 88.8 μg of b1s1e2-Fc WT. Seventy-two hours later, tumors were excised and analyzed via flow cytometry for count and percentage of $Foxp3^+$ $CD25^+$ (mean ± SD; $n = 5$). Statistics: transendocytosis assay compared by two-way ANOVA; cell counts and percentages compared by one-way ANOVA with Tukey's multiple comparisons test. n.s., not significant; $^{**}P < 0.01$; $^{****}P < 0.0001$.

B7.1 binding to CTLA-4 with an IC_{50} value of 24.4 nM (Fig. 2*D*). Since cell-surface CTLA-4 is less accessible than soluble CTLA-4-Fc, we were unsurprised to observe more blocking of B7.1 binding in the presence of b1s1e2-Fc than in the ELISA format, although with an IC_{50} value of 2.24 μM, b1s1e2-Fc required a two-log fold higher concentration than 9d9 to block B7.1.

CTLA-4 antagonism comprises both blockade of the CTLA-4:B7 axis and functionally inhibiting CTLA-4 from transendocytosing B7. To evaluate the impact of b1s1e2-Fc binding on B7 transendocytosis, we incubated recipient cells expressing CTLA-4 with donor cells expressing either B7.1 or B7.2 (C-terminally tagged with GFP) in the presence of various CTLA-4 binders. Following overnight incubation, the amount of remaining ligand on donor cells was measured to quantify transendocytosis. The amount of remaining ligand was equivalent in the presence of either b1s1e2-Fc or no antibody for both B7.1 (P = 0.9854) and B7.2 (P = 0.7634), confirming that b1s1e2-Fc does not functionally block CTLA-4 or inhibit transendocytosis (Fig. 2*E*). In contrast, the addition of 9d9 blocked transendocytosis and resulted in significantly increased amounts of both B7.1 (P = 0.0028) and B7.2 (P < 0.0001) remaining on donor cells. Representative histograms of donor cell GFP mean fluorescence intensity (MFI) are shown for each construct (Fig. 2*F*).

9d9 and b1s1e2-Fc Equivalently Deplete Intratumoral Tregs. The two anti-CTLA-4 therapies were tested for their ability to deplete intratumoral Tregs in vivo. Mice were subcutaneously inoculated with MC38 colon carcinoma tumors and dosed with molar equivalents of each construct either intraperitoneally (i.p.) or intratumorally (i.t.) on day 7 after tumor inoculation. Twenty-four hours later, tumors were excised and analyzed via flow cytometry. Both b1s1e2-Fc and 9d9 depleted intratumoral Tregs to equivalent levels both in count and as a percentage of $CD45^+$ cells when containing activating Fcs (WT) (Fig. 2*G* and *SI Appendix*, Fig. S3*A*). Total $CD45^+$, $CD3^+$, and $CD8^+$ counts remained unchanged or increased slightly, showing that this depletion was specific to Tregs (*SI Appendix*, Fig. S3*B*). We also harvested tumors 3 d after treatment to better understand the longevity of this Treg depletion, and we observed that the reduced intratumoral Treg levels were equivalently maintained for both b1s1e2-Fc WT and 9d9 WT (Fig. 2*H*). We also engineered silent Fc versions of both 9d9 and b1s1e2-Fc by introducing the LALA-PG mutations into the Fc to abrogate binding to FcγRs (69). The LALA-PG formats were unable to deplete Tregs, confirming that this is an FcγR-mediated phenomenon requiring an activating isotype (*SI Appendix*, Fig. S3*C*). We also observed similar trends of intratumoral Treg depletion using the B16/F10 melanoma model (*SI Appendix*, Fig. S3*D*).

9d9 WT Elicits More Long-Term Cures Than b1s1e2-Fc WT and 9d9 LALA-PG. Each construct was tested for therapeutic efficacy with both activating and silent Fc formats. Mice were subcutaneously inoculated with MC38 tumors, dosed with anti-CTLA-4 constructs either i.t. or i.p. on days 7, 10, and 14, and monitored for long-term survival (Fig. 3*A*). Mice dosed i.t. with either 9d9 WT or b1s1e2-Fc WT were afforded significant survival benefit over PBS-treated mice (P < 0.0001) (Fig. 3*B*). However, 9d9 WT resulted in significantly more cures than b1s1e2-Fc WT, with a cure rate of 47% (7 out of 15) compared to 0% (0 out of 8) (P = 0.0004). We also assessed the therapeutic efficacy of the LALA-PG formats, and 9d9 LALA-PG allowed us to evaluate the individual contribution of antagonism to efficacy. Consistent with previous literature, 9d9 LALA-PG afforded no survival over PBS (P = 0.2414), confirming that CTLA-4 antagonism is not an efficacious monotherapy (64). Because b1s1e2-Fc does not have the ability to antagonize CTLA-4, removing the ability to interact with FcγRs should completely abrogate any therapeutic capabilities, and we observed that b1s1e2-Fc LALA-PG did not provide any survival benefit over PBS (P = 0.8946).

We also dosed our constructs systemically (i.p.) at the same dose and schedule as the i.t. treatments since this is the clinical administration route for anti-CTLA-4 antibodies (Fig. 3*C*). Similar to the i.t. treatments, 9d9 WT and b1s1e2-Fc WT both afforded significant survival benefit over PBS (P < 0.0001). 9d9 WT again resulted in more cures than b1s1e2-Fc WT, with a cure rate of 33% (6 out of 18) compared to 10% (1 out of 10), although not significantly different (P = 0.5024). Once again, neither construct was efficacious in the LALA-PG format. None of the treatments caused weight loss over the course of the therapy (*SI Appendix*, Fig. S4*A*). The overall survival benefit from 9d9 WT was greater than that of either b1s1e2-Fc WT or 9d9 LALA-PG, demonstrating that the combination of CTLA-4 antagonism and intratumoral Treg depletion is synergistic and affords additional therapeutic efficacy compared to either function on its own.

9d9 Increases T Cell Priming in Tumor-Draining Lymph Nodes. To confirm that 9d9 treatment affords improved survival benefit compared to b1s1e2-Fc due to antagonism-mediated T cell priming, we looked in the tdLNs of mice following treatment. We inoculated mice with MC38 tumors, dosed on day 7, harvested tdLNs on day 10, and analyzed the tissues via flow cytometry (Fig. 3*D*). Just 3 d later, the percentage of $CD4^+$ and $CD8^+$ effector T cells expressing proliferation marker Ki67 and activation marker PD-1 increased in 9d9-treated mice compared to PBS, whereas there was no change in b1s1e2-Fc-treated mice (Fig. 3 *E* and *F*). Although we did not observe any significant changes in the counts of these cells at this time point, they were trending upward in the 9d9-treated group. Additionally, 9d9 treatment increased the count and percentage of $Ki67^+$ Tregs in the tdLN compared to PBS and b1s1e2-Fc (although we did not observe significant differences in PD-1 expression), in agreement with previous literature (Fig. 3*G* and *SI Appendix*, Fig. S4*B*) (61, 62). The evidence of broad T cell priming and activation in the tdLNs of 9d9-treated mice but not b1s1e2-Fc-treated mice confirms that CTLA-4 antagonism is required for anti-CTLA-4 antibodies to enhance priming of T cells. Taken with our survival data, we demonstrate that this resultant T cell priming contributes to and is essential for maximum antitumor efficacy of anti-CTLA-4 therapies.

Intratumoral Tregs Express More CTLA-4 Than Other Tregs. Although 9d9 treatment caused nodal Treg expansion 3 d later, we also looked 1 d after treatment with either 9d9 or b1s1e2-Fc to confirm that there was no transient nodal Treg depletion in either the MC38 or B16/F10 tumor model (Fig. 4*A* and *SI Appendix*, Fig. S4*C*). Tregs in the TME have been previously shown to express higher levels of surface CTLA-4 than Tregs in other compartments (64). To confirm this, we measured the percentage of Tregs expressing detectable levels of surface CTLA-4 and the MFIs of surface and total (surface and intracellular) CTLA-4 since 90% of CTLA-4 resides intracellularly. Consistent with previous literature, we observed that in PBS-treated mice, both the percentage of $CTLA\text{-}4^+$ Tregs and the level of CTLA-4 expression were substantially higher for Tregs in the tumor compared to the tdLN (Fig. 4 *B* and *C*). Since nodal Tregs lack sufficient CTLA-4 expression for Fc-mediated depletion, treatment with 9d9 results in the priming of these Tregs along with the other nodal T cell populations. We also found that in mice treated with either 9d9

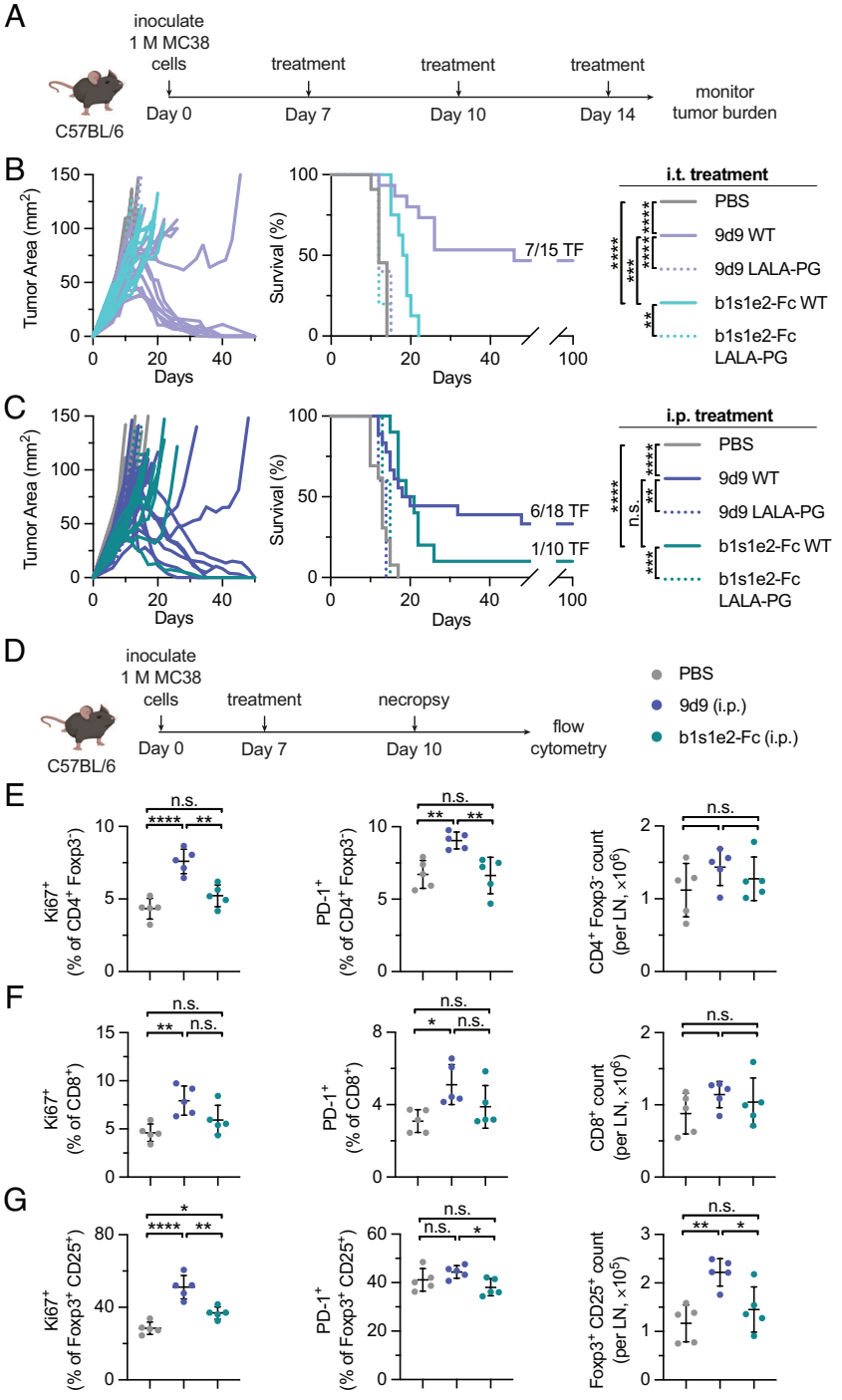

Fig. 3. Survival benefit and priming effects of b1s1e2-Fc and 9d9 in vivo. (*A*) MC38-bearing mice were treated either i.p. or i.t. on days 7, 10, and 14 with PBS, 200 μg of 9d9, or 88.8 μg of b1s1e2-Fc (molar equivalent). (*B*) Individual tumor growth curves (*B*, *Left*) and survival (*B*, *Right*) for mice treated i.t.; PBS (n = 11); 9d9 WT (n = 15); 9d9 LALA-PG (n = 5); b1s1e2-Fc WT (n = 8); b1s1e2-Fc LALA-PG (n = 5). (*C*) Individual tumor growth curves (*C*, *Left*) and survival (*C*, *Right*) for mice treated i.p.; PBS (n = 13); 9d9 WT (n = 18); 9d9 LALA-PG (n = 5); b1s1e2-Fc WT (n = 10); b1s1e2-Fc LALA-PG (n = 5). (*D*) MC38-bearing mice were treated i.p. on day 7 with PBS, 9d9 WT, or b1s1e2-Fc WT. On day 10, tdLNs were excised and analyzed via flow cytometry. (*E*) Percentage Ki67$^+$, PD-1$^+$, and total count per LN of CD4$^+$ Foxp3$^-$ T cells (gated on single cell/live/CD45$^+$/CD3$^+$) (mean ± SD; n = 5). (*F*) Percentage Ki67$^+$, PD-1$^+$, and total count per LN of CD8$^+$ T cells (gated on single cell/live/CD45$^+$/CD3$^+$) (mean ± SD; n = 5). (*G*) Percentage Ki67$^+$, PD-1$^+$, and total count per LN of Foxp3$^+$ CD25$^+$ Tregs (gated on single cell/live/CD45$^+$/CD3$^+$/CD4$^+$) (mean ± SD; n = 5). Statistics: survival compared by the log-rank Mantel-Cox test.; cell counts and percentages compared by one-way ANOVA with Tukey's multiple comparisons test. n.s., not significant; *P < 0.05; **P < 0.01; ***P < 0.001; ****P < 0.0001.

or b1s1e2-Fc, the remaining intratumoral Tregs expressed very low levels of CTLA-4, as well as IFNγ, PD-1, and granzyme B (*SI Appendix*, Fig. S4*D*). These Tregs not only express insufficient surface CTLA-4 for Fc-mediated depletion but also lack the canonical immunosuppressive phenotype that characterizes intratumoral Tregs, suggesting that they have just infiltrated the tumor and not yet upregulated CTLA-4 in response to the immunosuppressive environment.

Intratumoral DT Is Efficacious in Foxp3-DTR Mice. While 9d9 provided priming benefits in the tdLN compared to b1s1e2-Fc through CTLA-4 antagonism, this priming was not limited to the effector T cell compartment. In fact, Tregs expanded to a greater degree than effector T cells 72 h after treatment (Fig. 3 *E*–*G*), likely due to their higher CTLA-4 expression (*SI Appendix*, Fig. S4 *E* and *F*). Since Tregs are known to restrain priming in the tdLN, this nodal Treg expansion following 9d9 treatment is partially counteracting the priming of effector T cells (31–35). Therefore, we hypothesized that a therapy which depletes nodal Tregs, in addition to intratumoral Tregs, would result in superior effector T cell priming and have even greater antitumor efficacy than 9d9. To test this, we employed the Foxp3-DTR mouse model as a system for CTLA-4-agnostic Treg depletion. To avoid the lethal autoimmunity these mice experience with systemic DT administration, we developed a low-dose, i.t. dosing schedule to achieve local (tumor and tdLN) Treg depletion while minimizing systemic depletion (35–37, 41). To validate our approach, we administered three doses of DT: 75 ng (i.t.), 125 ng (i.t.), or 1 μg

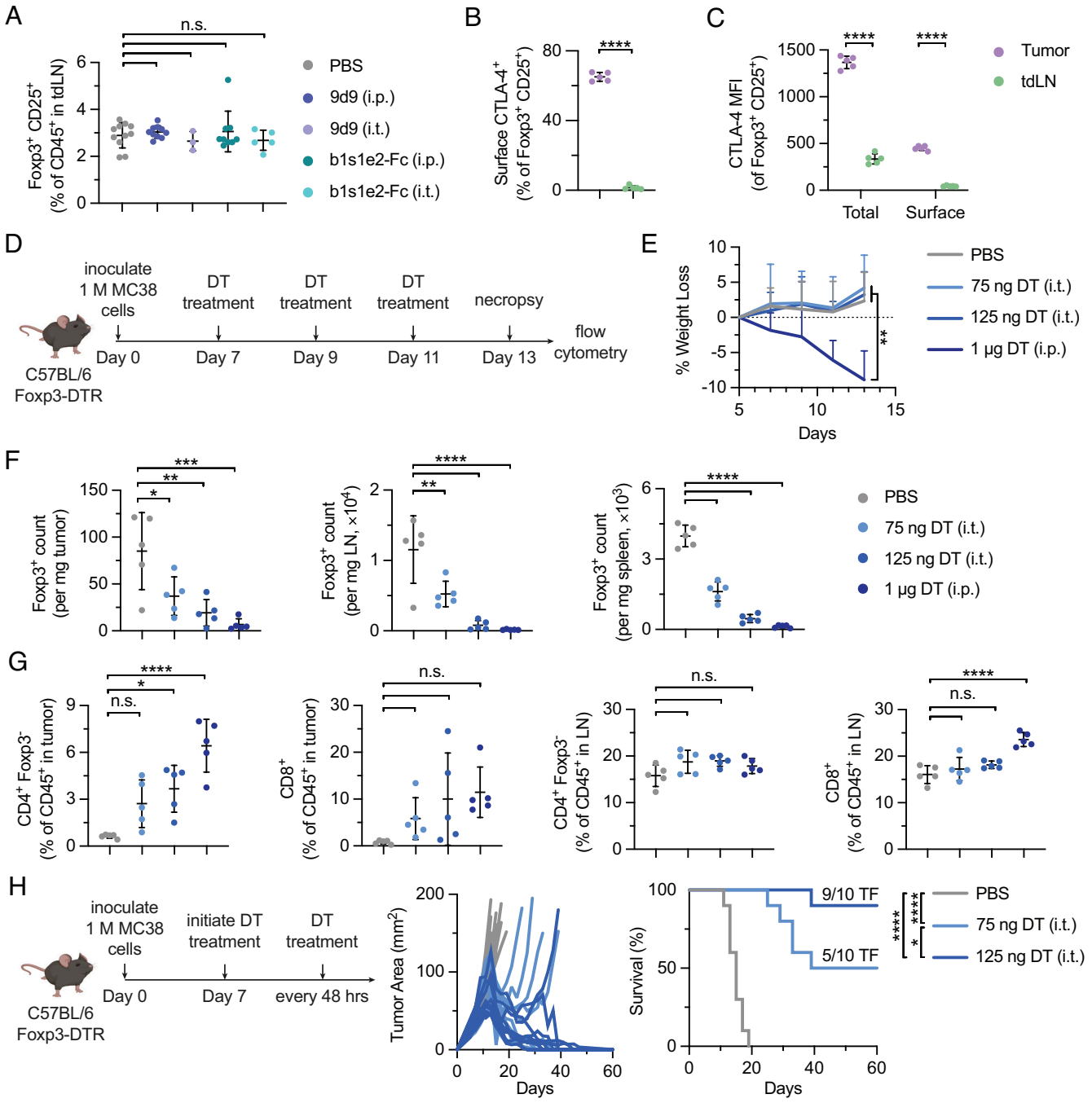

Fig. 4. Antitumor efficacy of combined intratumoral and nodal Treg depletion with diphtheria toxin treatment in Foxp3-DTR mice. (*A*) MC38-bearing mice were treated either i.p. or i.t. on day 7 with PBS, 200 µg of 9d9, or 88.8 µg of b1s1e2-Fc (molar equivalent). On day 8, tdLNs were excised and analyzed via flow cytometry. Percentage of Foxp3$^+$ CD25$^+$ Tregs in the tdLN (gated on single cell/live/CD45$^+$/CD3$^+$) (mean ± SD; n = 3 to 14). (*B* and *C*) On day 10, tumors and tdLNs of MC38-bearing mice treated i.p. with PBS were excised and analyzed via flow cytometry. (*B*) Percentage of Foxp3$^+$ CD25$^+$ Tregs that were surface CTLA-4$^+$ (gated on single cell/live/CD45$^+$/CD3$^+$/CD4$^+$) (mean ± SD; n = 5). (*C*) Total and surface CTLA-4 MFI of Foxp3$^+$ CD25$^+$ Tregs (gated on single cell/live/CD45$^+$/CD3$^+$/CD4$^+$) (mean ± SD; n = 5). (*D*) MC38-bearing Foxp3-DTR mice were treated with PBS, 75 ng DT (i.t.), 125 ng DT (i.t.), or 1 µg DT (i.p.) on days 7, 9, and 11. On day 13, tumors, tdLNs, and spleens were excised and analyzed via flow cytometry. Mice were monitored for weight loss until euthanasia. (*E*) Treatment schedule as described in *D*. Body weight normalized to day 5, significance comparisons for normalized body weight at day 13 (n = 5). (*F*) Treatment schedule as described in *D*. Count of Foxp3$^+$ Tregs per mg tumor, LN, and spleen (gated on single cell/live/CD45$^+$/CD3$^+$/CD4$^+$) (mean ± SD; n = 5). (*G*) Treatment schedule as described in *D*. Percentage of CD4$^+$ Foxp3$^-$ and CD8$^+$ T cells in the tumor and tdLN (gated on single cell/live/CD45$^+$/CD3$^+$) (mean ± SD; n = 5). (*H*) MC38-bearing Foxp3-DTR mice were treated i.t. with PBS, 75 ng DT, or 125 ng DT every 48 h starting on day 7 until cured or killed. Individual tumor growth curves and survival (n = 10, data combined from two different experiments). Statistics: survival compared by the log-rank Mantel-Cox test; CTLA-4 MFI and weight loss compared by two-way ANOVA; cell counts and percentages compared by one-way ANOVA with Tukey's multiple comparisons test; CTLA-4$^+$ Tregs compared by the unpaired t test. n.s., not significant; *P < 0.05; **P < 0.01; ***P < 0.001; ****P < 0.0001.

(i.p.) (Fig. 4*D*). Encouragingly, both low-dose i.t. groups did not experience any weight loss compared to PBS-treated mice, whereas the 1 µg systemically dosed mice showed significant weight loss (Fig. 4*E*). Additionally, the degree of Treg depletion in the tumor, tdLN, and spleen was directly proportional to the amount of DT dosed, with all three doses selectively depleting Tregs compared to PBS-treated mice (Fig. 4*F* and *SI Appendix*, Fig. S5*A*). We also evaluated the amount of effector T cells in the tumor and tdLN as a metric for enhanced priming (Fig. 4*G*). The percentage of intratumoral CD4$^+$ effector T cells increased proportionally with

the DT dose administered, compared to PBS-treated mice. The percentage of $CD8^+$ T cells in the tumor also trended upward proportionally to dose, but this result was not statistically significant. The percentages of $CD4^+$ and $CD8^+$ effector T cells in the tdLN were largely unchanged, except for the 1 μg treated mice, which had increased percentages of $CD8^+$ effector T cells.

To evaluate this combined intratumoral and nodal Treg depletion strategy in a therapeutic context, we subcutaneously inoculated Foxp3-DTR mice with MC38 tumors and initiated DT administration on day 7 (Fig. 4*H*). To ensure that Tregs were continuously and consistently depleted, mice were dosed every 48 h from the start of treatment until either no palpable tumor was detectable or the mouse reached euthanasia criteria. We excluded the 1 μg systemic group from this study since it is already established that mice treated at this dose will die from autoimmunity independent of tumor burden. Treatment with 125 ng of DT resulted in 90% survival (9 out of 10) compared to 75 ng of DT resulting in 50% survival (5 out of 10) with both doses providing significant survival benefit over PBS ($P < 0.0001$). Additionally, this long-term, local Treg depletion did not cause any weight loss throughout the course of treatment (*SI Appendix*, Fig. S5*B*). Similar trends have been reported in the less immunogenic B16/F10 model, although with lower cure rates (35). The high cure rates resulting from this local DT dosing schedule demonstrate that combined intratumoral and nodal Treg depletion can offer advantages over the use of agents that nonspecifically prime all nodal T cells, including Tregs, and is a promising therapeutic approach.

Discussion

While the mechanism of action of anti-CTLA-4 antibodies has been explored for over a decade, there is still a great deal of uncertainty surrounding the contributions of antagonism and Treg depletion. In mice, Treg depletion has been confirmed as an essential component of anti-CTLA-4 therapies, but controversy remains regarding a requirement for CTLA-4 antagonism. To answer this question, we developed an anti-CTLA-4 binder with the ability to deplete intratumoral Tregs without antagonizing CTLA-4. We found that Treg depletion is agnostic of the CTLA-4 binding epitope and observed equivalent levels of intratumoral Treg depletion for the antagonistic and nonantagonistic constructs. 9d9 WT outperformed both b1s1e2-Fc WT and 9d9 LALA-PG therapeutically, demonstrating that both Treg depletion and CTLA-4 antagonism are essential for maximum antitumor efficacy of anti-CTLA-4 therapies.

The lack of therapeutic efficacy of 9d9 LALA-PG, the construct capable of antagonism only, leaves no doubt that Treg depletion is essential for efficacy in this system, confirming previous reports (63–67). The comparison of 9d9 WT, the only construct capable of both antagonism and Treg depletion, to b1s1e2-Fc WT shows that the two mechanisms are synergistic and only therapies with both functions result in the highest antitumor efficacy. The synergism of the two mechanisms suggests that the priming benefit in the tdLN afforded by CTLA-4 antagonism is not able to provide antitumor benefit without intratumoral Treg depletion and vice versa. We hypothesize that in the absence of intratumoral Treg depletion, newly primed effector T cells traffic to the tumor but are unable to function properly in the presence of high intratumoral Treg numbers. Similarly, treatment with b1s1e2-Fc WT depletes intratumoral Tregs and remodels the immunosuppressive TME landscape, but without any additional priming in the tdLN, there are insufficient numbers of effector T cells trafficking to the tumor. Only in the group treated with 9d9 WT do we observe consistent and robust tumor control in a high proportion of mice, demonstrating that the combination of enhanced T cell priming and intratumoral Treg depletion leads to the efficacy of anti-CTLA-4 antibodies.

The ability of anti-CTLA-4 antibodies to deplete intratumoral Tregs in humans is highly contested; however, until recently, the only approved anti-CTLA-4 antibody, ipilimumab, was of the activating isotype (hIgG1), which is capable of eliciting ADCC/P. On the other hand, tremelimumab (hIgG2) is not of the activating isotype and failed to be approved as a monotherapy. In October 2022, it was approved in combination with durvalumab (anti-PD-L1) for unresectable hepatocellular carcinoma. This supports the idea that antagonism alone is insufficient to mount a proper antitumor immune response. The overwhelming body of evidence supporting the benefit of Treg depletion to anti-CTLA-4 antibodies in mice has sparked efforts to improve the Treg-depleting capabilities of human anti-CTLA-4 antibodies. There are ongoing clinical trials for botensilimab, an Fc-engineered anti-CTLA-4 antibody with improved Treg depletion capabilities. A recent preclinical study combined anti-CTLA-4 therapy with Toll-like receptor 1/2 ligand to increase FcγR expression and enhance intratumoral Treg depletion (79). Our work supports the development and use of anti-CTLA-4 antibodies with robust Treg depletion capabilities but suggests developing approaches to expand this depletion beyond the tumor.

While 9d9 WT outperformed all other anti-CTLA-4 constructs tested in this work, it still only cured less than 50% of mice, which we believe is related to the nonspecificity of the T cell priming in the tdLNs. An important functional consequence of CTLA-4 antagonism in the tdLN is the reduction of B7 transendocytosis, which allows for enhanced priming of all nodal T cell populations. Since nodal Treg CTLA-4 expression is much lower than that of their intratumoral counterparts, rather than observing their depletion following anti-CTLA-4 therapy, this Treg population experiences enhanced costimulation and subsequent expansion along with the effector T cell populations. This proliferative Treg phenotype is also seen in $CTLA\text{-}4^{-/-}$ mice, confirming that 9d9, but not b1s1e2-Fc, blocks CTLA-4, allowing for increased CD28 signaling and enhanced Treg activation (80). The expansion of nodal Tregs as a result of CTLA-4 blockade may allow for Treg functions to dominate the antitumor immune response. Therefore, while the priming resulting from CTLA-4 antagonism is net beneficial and essential for efficacy, we believe that superior tumor control could be achieved if priming in the tdLN was specific to effector T cells or nodal Tregs were also depleted.

As proof of concept, our i.t., low-dose DT administration in Foxp3-DTR mice demonstrates the powerful antitumor efficacy that combined intratumoral and nodal Treg depletion can achieve. This system provides clear mechanistic evidence that supports the idea that nodal Tregs are preventing anti-CTLA-4 antibodies from obtaining their full therapeutic potential (35). In the absence of CTLA-4 antagonism, DT-mediated nodal Treg depletion indirectly provides priming benefits, as shown by increased effector T cells in the tumor following treatment. DT treatment resulted in higher cure rates than any anti-CTLA-4 therapy tested in this work, providing a framework for avenues of improvement upon current therapies. However, outside of the Foxp3-DTR model, targeting nodal Tregs remains a significant challenge. One potential approach is the use of anti-CD25 antibodies to leverage the differential expression of CD25 on Tregs compared to effector T cells, but similarly to CTLA-4, intranodal Tregs express less CD25 than intratumoral Tregs and equivalent levels to circulating Tregs (81). While anti-CD25 mIgG2a administration provides robust intratumoral Treg depletion, it only reduces nodal Tregs by about half and equivalently reduces circulating Tregs. Anti-CD25

antibodies have been further improved to preserve IL-2-STAT5 signaling, but ultimately, traditional Fc-mediated Treg depletion using targets expressed equivalently on nodal and systemic Tregs is constrained by concerns of severe toxicity (82).

Clinical evidence for the development of therapies that deplete nodal Tregs shows that in patients, higher Treg levels in tdLNs and tertiary lymphoid structures are more highly correlated with disease progression than intratumoral Tregs in some contexts (18, 83). This correlation is likely due to either enhanced Treg-mediated restraint of effector T cell priming or larger reservoirs of Tregs that traffic to the tumor (28, 33, 84). Depletion of nodal Tregs in mice has been shown to disrupt nodal architecture, expand the T cell zone, increase development of high endothelial venules, and enhance cytotoxic T cell priming, proliferation, and trafficking to the tumor (28, 85, 86). One way in which Tregs self-regulate their proliferation is via TGF-β, and inhibition of TGF-β in the tdLN reduces Treg proliferation and increases IFNγ-producing effector T cells (87). Our work supports the notion that nodal Treg depletion increases effector T cell trafficking to the tumor and that the combination of intratumoral and nodal Treg depletion results in powerful antitumor efficacy.

In conclusion, we demonstrate that anti-CTLA-4 antibodies with only the ability to either deplete intratumoral Tregs or antagonize CTLA-4 are not efficacious as monotherapies. Rather, our data provide compelling evidence that both proposed mechanisms for anti-CTLA-4 antibodies are synergistic and their combination results in the greatest antitumor efficacy. Our work with low-dose, intratumoral DT shows that nodal Tregs are restraining priming in the tdLN and that their depletion leads to even greater antitumor efficacy than current anti-CTLA-4 antibodies can provide. The lack of CTLA-4 expression on these nodal Tregs suggests that alternative strategies should be employed to deplete them. This nodal Treg depletion, when combined with anti-CTLA-4 antibodies or other immunotherapies, has the potential to provide antitumor immune responses beyond that of current anti-CTLA-4 therapies.

Materials and Methods

Mice. B6 (C57BL/6NTac) mice were purchased from Taconic. B6 Foxp3-DTR (B6.129(Cg)-*Foxp3*$^{tm3(DTR/GFP)Ayr}$/J) mice were a gift from the Spranger lab, bred in house, and genotyped using Transnetyx. Six- to eight-week-old females were used in experiments. All animal work was conducted under the approval of the Massachusetts Institute of Technology Committee on Animal Care in accordance with federal, state, and local guidelines.

Cells. MC38 cells (a gift from J. Schlom, National Cancer Institute, Bethesda, MD) and B16/F10 [American Type Culture Collection (ATCC)] cells were cultured in Dulbecco's modified Eagle's medium (ATCC) supplemented with 10% fetal bovine serum (Gibco) at 37 °C and 5% CO_2. HEK293-F cells (Gibco) were cultured in FreeStyle293 Expression Medium (Gibco) shaking at 37 °C and 8% CO_2. CTLA-4 expressing stable lines were made by transfecting HEK293-F cells with the PiggyBac system (System Biosciences) and sorting GFP$^+$ cells on a FACS Aria III Cell Sorter (BD). Sorted cells were cultured in the presence of 100 units/mL of penicillin and 100 μg/mL of streptomycin (Gibco) for 3 d. CHO DG44 cells were cultured in ProCHO5 (Lonza) supplemented with 4 mM L-glutamine, 0.1 mM hypoxanthine, and 16 μM thymidine shaking at 37 °C and 8% CO_2. 9d9 mIgG2c WT producing stable lines were made by transfecting CHO DG44 cells with the PiggyBac system (System Biosciences) and gifted to us from David Hacker. All cell lines tested negative for mycoplasma.

Yeast Surface Display. Yeast surface display was performed using standard methods as described elsewhere (68). Briefly, CTLA-4 binders were sorted from two previously developed libraries (71, 72). Yeast libraries were grown in SD-CAA at 30 °C and induced in SG-CAA overnight at 20 °C. Yeast incubations were performed in PBSA [Phosphate-buffered saline (PBS, Corning) + 0.1% bovine serum albumin (BSA, Sigma Aldrich)] at room temperature (RT). Naive libraries were sorted using magnetic bead selections followed by FACS. Affinity maturation was performed by mutagenesis of identified binder sequences, library generation, and subsequent sorting using standard methods as described elsewhere (74). Mutagenesis of sequences was performed using error-prone PCR (epPCR), and libraries were generated using two-piece homologous recombination in yeast. The resulting libraries were grown, induced, sorted via FACS, and sequenced as before. The CTLA-4 YSD library was also created using epPCR, and epitope mapping was performed using alternating FACS negative selections for the binder of interest and positive selections for a binder with a nonoverlapping epitope. Additional details are provided in *SI Appendix*.

Cloning and Protein Purification. Murine CTLA-4-Fc, B7.1-Fc, CD28-Fc, b1s1e2-Fc, b1h1e3 mIgG2c, and 9d9 mIgG2c LALA-PG were cloned into the gWiz vector (Genlantis) using In-Fusion cloning (Takara) (*SI Appendix*, Table S4). The cysteines in the hinge regions of CTLA-4-Fc, B7.1-Fc, and CD28-Fc were mutated to serines to allow for the protein to guide dimerization (3). b1h1e3 was expressed as a chimeric antibody with human variable regions and the murine IgG2c and kappa light chain constant regions. b1s1e2-Fc and b1h1e3 were cloned as activating (WT) and silent [with the LALA-PG mutations to ablate FcγR binding (69)] formats. Plasmids for transient expression of CTLA-4 on the surface of HEK293-F cells were cloned using In-Fusion (Takara) into the pIRES vector, which encodes for GFP downstream of the CTLA-4 gene, separated by an internal ribosome entry site (IRES) site. Plasmids were amplified in Stellar cells (*Escherichia coli*) and purified using NucleoBond Xtra endotoxin-free kits (Macherey-Nagel). For all proteins except 9d9 mIgG2c WT, HEK293-F cells were transiently transfected with 1 mg/L plasmid DNA, 2 mg/L polyethylenimine (Polysciences), and 40 mL/L OptiPRO Serum Free Medium (Thermo Fisher), added dropwise. For 9d9 mIgG2c WT, the CHO DG44 stable production line was seeded at a density of 0.5 M/mL. After 6 d for transiently transfected proteins or 10 d for the stable production line, proteins were purified from cell supernatants using rProtein A Sepharose Fast Flow Resin (Cytiva). Proteins were buffer exchanged into PBS (Corning) using Amicon filters (Millipore Sigma). Proteins were sterile filtered and confirmed for minimal endotoxin (<0.1 EU/dose) using the Endosafe LAL Cartridge Technology (Charles River). Molecular weight was confirmed with sodium dodecyl-sulfate polyacrylamide gel electrophoresis (SDS-PAGE, Invitrogen). Proteins were run alongside the Novex Sharp Pre-Stained Protein Standard (Invitrogen) on a NuPAGE 4 to 12% Bis-Tris gel (Invitrogen) with 2-(*N*-morpholino) ethanesulfonic acid (MES) running buffer and stained for visualization with SimplyBlue Safe Stain (Life Technologies).

Equilibrium and Competition Binding Assays. HEK293-F cells transiently expressing surface CTLA-4 were transfected as previously described 24 to 48 h prior to incubations. HEK293-F cells (either stably or transiently expressing surface CTLA-4) were incubated with titrations of proteins for 2 h at 37 °C and with a constant concentration of B7.1-Fc for 1 additional hour for the competition assays. Cells were stained for viability, washed with PBSA, and analyzed with a FACS Symphony A3 (BD). Additional details are provided in *SI Appendix*.

ELISA. Clear Flat-bottom Immuno Nonsterile Nunc 96-well MaxiSorp Plates (Invitrogen) were coated overnight at 4 °C. Wells were washed twice with PBST [PBS + 0.1% vol/vol Tween-20 (Millipore Sigma)] and then blocked with PBSTA (PBS + 0.2% wt/vol BSA + 0.1% vol/vol Tween-20) for 2 h at RT. Subsequent binding incubations were performed for 30 min-3 h at RT in PBSTA, and wells were washed 5 times with PBST. 1-Step Ultra TMB-ELISA Substrate Solution (Thermo Fisher) was added for 5 to 10 min, followed by 1 M sulfuric acid to stop the chromogenic reaction. Absorbance at 450 nm (corrected with a reference absorbance at 570 nm) was measured on an Infinite M200 microplate reader (Tecan). Additional details are provided in *SI Appendix*.

Transendocytosis Assay. Cell line engineering and assay conditions were performed as described elsewhere (88). Briefly, ligand donor cells were CHO cells stably expressing CD80 or CD86 molecules C-terminally tagged with GFP. Donor cells were labeled with CellTrace Violet (Thermo Fisher). CHO cells stably expressing CTLA-4^{WT} and cytoplasmic mCherry were used as recipient cells. Donor and recipient cells or CTLA$^-$ control cells were plated in round-bottomed, 96-well plates at 37 °C at the ratio of 3:1 donor to recipient cells overnight. Cells were then disaggregated by pipetting and analyzed by flow cytometry. Transendocytosis was

quantified by GFP signal on donor cells compared to that of donor cells incubated with CTLA-4$^-$ control cells.

Tumor Treatments and Survival. On day 0, mice were inoculated with 1 M MC38 cells in 50 µL PBS subcutaneously in the right flank. Treatments began on day 7 when tumors were established. Mice were sorted such that each group had an equal average tumor area at the start of treatment. Mice were treated with 200 µg 9d9 or 88.8 µg b1s1e2-Fc (molar equivalent) on days 7, 10, and 14. DT (Sigma) was dissolved in PBS to a concentration of 1 mg/mL. Aliquots were flash-frozen in liquid nitrogen and stored at −80 °C. Right before dosing, DT was thawed on ice and diluted in PBS to the appropriate concentrations. DT was dosed every 48 h starting on day 7 until the mouse was cured (no palpable tumor was detectable) or reached the euthanasia criteria (35). I.p. doses were given in 100 µL PBS, and i.t. doses were given in 20 µL PBS. Tumor area (length × width) and body weight were monitored every 2 to 3 d. Most survival data are compiled from multiple experiments. Mice were killed when tumors exceeded 100 mm^2 (or 150 mm^2 for Foxp3-DTR mouse experiments) or exhibited poor body condition. All cured Foxp3-DTR mice were killed at day 60.

Flow Cytometry. Tumors were excised, weighed, mechanically dissociated, enzymatically digested and dissociated, and filtered into single-cell suspensions. Spleens and tdLNs were excised, weighed, mechanically dissociated, and filtered into single-cell suspensions. Red blood cells were removed from spleen samples using the ACK lysing buffer (Gibco). Cells were stained for viability and extracellular markers, fixed and permeabilized, stained for intracellular markers, and resuspended in PBSA for flow cytometry. Additional details are provided in *SI Appendix*.

Statistical Analysis. Statistics were performed with GraphPad Prism software V9. Survival was compared by the log-rank Mantel-Cox test. As described in figure captions, other metrics were compared by one-way or two-way (ANOVA) with Tukey's multiple comparisons test or unpaired *t* test. Samples identified as outliers using the ROUT test with Q = 1% were removed. The *n* and *P* values are indicated in the figure captions.

Data, Materials, and Software Availability. All study data are included in the article and/or *SI Appendix*.

ACKNOWLEDGMENTS. This work was supported by CA271243 and EB031082. B.M.L., J.R.P., E.A.L., A.S., L.S., and A.M.R. were supported by the NSF Graduate Research Fellowship Program. L.D. was supported by the Ludwig Center at the Koch Institute. We thank the Koch Institute's Robert A. Swanson (1969) Biotechnology Center (National Cancer Institute Grant P30-CA14051) for technical support, specifically the Flow Cytometry Core Facility. We thank the Protein Production and Structure Core Facility at the École polytechnique fédérale de Lausanne for the development of the 9d9 stable line. We thank the Spranger lab for the gift of the Foxp3-DTR breeding pair. Biorender was used to make some of the schematics.

Author affiliations: [a]Koch Institute for Integrative Cancer Research, Massachusetts Institute of Technology, Cambridge, MA 02139; [b]Department of Chemical Engineering, Massachusetts Institute of Technology, Cambridge, MA 02139; [c]Department of Biological Engineering, Massachusetts Institute of Technology, Cambridge, MA 02139; [d]Institute of Immunity and Transplantation, University College London, London NW3 2PP, United Kingdom; and [e]Department of Biology, Massachusetts Institute of Technology, Cambridge, MA 02139

Author contributions: B.M.L. and K.D.W. designed research; B.M.L., J.R.P., E.A.L., A.S., J.A.S., L.D., L.S., and A.K. performed research; A.K., A.M.R., S.S., and D.M.S. contributed new reagents/analytic tools; B.M.L., J.R.P., A.K., S.S., D.M.S., and K.D.W. analyzed data; and B.M.L. and K.D.W. wrote the paper.

1. S. Read, V. Malmström, F. Powrie, Cytotoxic T lymphocyte-associated antigen 4 plays an essential role in the function of $CD25^+$ $CD4^+$ regulatory cells that control intestinal inflammation. *J. Exp. Med.* **192**, 295–302 (2000).
2. T. Takahashi *et al.*, Immunologic self-tolerance maintained by $CD25^+CD4^+$ regulatory T cells constitutively expressing cytotoxic T lymphocyte-associated antigen 4. *J. Exp. Med.* **192**, 303–310 (2000).
3. P. S. Linsley *et al.*, CTLA-4 is a second receptor for the B cell activation antigen B7. *J. Exp. Med.* **174**, 561–569 (1991).
4. S. Ikemizu *et al.*, Structure and dimerization of a soluble form of B7–1. *Immunity* **12**, 51–60 (2000).
5. T. Pentcheva-Hoang, J. G. Egen, K. Wojnoonski, J. P. Allison, B7–1 and B7–2 selectively recruit CTLA-4 and CD28 to the immunological synapse. *Immunity* **21**, 401–413 (2004).
6. O. S. Qureshi *et al.*, Trans-endocytosis of CD80 and CD86: A molecular basis for the cell-extrinsic function of CTLA-4. *Science* **332**, 600–603 (2011).
7. V. Ovcinnikovs *et al.*, CTLA-4–mediated transendocytosis of costimulatory molecules primarily targets migratory dendritic cells. *Sci. Immunol.* **4**, eaaw0902 (2019).
8. S. Hori, T. Nomura, S. Sakaguchi, Control of regulatory T cell development by the transcription factor foxp3. *Science* **299**, 1057–1061 (2003).
9. J. D. Fontenot, M. A. Gavin, A. Y. Rudensky, Foxp3 programs the development and function of $CD4^+CD25^+$ regulatory T cells. *Nat. Immunol.* **4**, 330–336 (2003).
10. K. Wing *et al.*, CTLA-4 control over $foxp3^+$ regulatory T cell function. *Science* **322**, 271–275 (2008).
11. R. H. Friedline *et al.*, $CD4^+$ regulatory T cells require CTLA-4 for the maintenance of systemic tolerance. *J. Exp. Med.* **206**, 421–434 (2009).
12. X. Tai *et al.*, Basis of CTLA-4 function in regulatory and conventional $CD4^+$ T cells. *Blood* **119**, 5155–5163 (2012).
13. P. Waterhouse *et al.*, Lymphoproliferative disorders with early lethality in mice deficient in Ctla-4. *Science* **270**, 985–988 (1995).
14. E. A. Tivol *et al.*, Loss of CTLA-4 leads to massive lymphoproliferation and fatal multiorgan tissue destruction, revealing a critical negative regulatory role of CTLA-4. *Immunity* **3**, 541–547 (1995).
15. T. J. Curiel *et al.*, Specific recruitment of regulatory T cells in ovarian carcinoma fosters immune privilege and predicts reduced survival. *Nat. Med.* **10**, 942–949 (2004).
16. G. J. Bates *et al.*, Quantification of regulatory T cells enables the identification of high-risk breast cancer patients and those at risk of late relapse. *J. Clin. Oncol.* **24**, 5373–5380 (2006).
17. J. Shou, Z. Zhang, Y. Lai, Z. Chen, J. Huang, Worse outcome in breast cancer with higher tumor-infiltrating $Foxp3^+$ Tregs: A systematic review and meta-analysis. *BMC Cancer* **16**, 687 (2016).
18. P. Devi-Marulkar *et al.*, Regulatory T cells infiltrate the tumor-induced tertiary lymphoïd structures and are associated with poor clinical outcome in NSCLC. *Commun. Biol.* **5**, 1416 (2022).
19. L. Strauss *et al.*, A unique subset of $CD4^+$ CD25high $Foxp3^+$ T cells secreting interleukin-10 and transforming growth factor-β1 mediates suppression in the tumor microenvironment. *Clin. Cancer Res.* **13**, 4345–4354 (2007).
20. M. E. Turnis *et al.*, Interleukin-35 limits anti-tumor immunity. *Immunity* **44**, 316–329 (2016).
21. D. V. Sawant *et al.*, Adaptive plasticity of IL-10^+ and IL-35^+ Treg cells cooperatively promotes tumor T cell exhaustion. *Nat. Immunol.* **20**, 724–735 (2019).
22. W. Chen *et al.*, Conversion of peripheral $CD4^+$ $CD25^-$ naive T cells to $CD4^+$ $CD25^+$ regulatory T cells by TGF-β induction of transcription factor foxp3. *J. Exp. Med.* **198**, 1875–1886 (2003).
23. C. A. Stewart *et al.*, Interferon-dependent IL-10 production by tregs limits tumor Th17 inflammation. *J. Clin. Invest.* **123**, 4859–4874 (2013).
24. A. Śledzińska *et al.*, Regulatory T cells restrain interleukin-2- and blimp-1-dependent acquisition of cytotoxic function by $CD4^+$ T cells. *Immunity* **52**, 151–166 (2020).
25. E. N. Scott, A. M. Gocher, C. J. Workman, D. A. A. Vignali, Regulatory T cells: Barriers of immune infiltration into the tumor microenvironment. *Front. Immunol.* **12**, 702–726 (2021).
26. D. H. Munn, A. L. Mellor, The tumor-draining lymph node as an immune-privileged site. *Immunol. Rev.* **213**, 146–158 (2006).
27. Z. Liu, J. H. Kim, L. D. Falo, Z. You, Tumor regulatory T cells potently abrogate antitumor immunity. *J. Immunol.* **182**, 6160–6167 (2009).
28. N. S. Joshi *et al.*, Regulatory T cells in tumor-associated tertiary lymphoid structures suppress anti-tumor T cell responses. *Immunity* **43**, 579–590 (2015).
29. R. Alonso *et al.*, Induction of anergic or regulatory tumor-specific $CD4^+$ T cells in the tumor-draining lymph node. *Nat. Commun.* **9**, 2113 (2018).
30. T. Hiura *et al.*, Both regulatory T cells and antitumor effector T cells are primed in the same draining lymph nodes during tumor progression. *J. Immunol.* **175**, 5058–5066 (2005).
31. M.-L. Chen *et al.*, Regulatory T cells suppress tumor-specific CD8 T cell cytotoxicity through TGF-β signals in vivo. *Proc. Natl. Acad. Sci. U.S.A.* **102**, 419–424 (2005).
32. A. Boissonnas *et al.*, $Foxp3^+$ T cells induce perforin-dependent dendritic cell death in tumor-draining lymph nodes. *Immunity* **32**, 266–278 (2010).
33. T. B. Shabaneh *et al.*, Oncogenic BRAFV600E governs regulatory T cell recruitment during melanoma tumorigenesis. *Cancer Res.* **78**, 5038–5049 (2018).
34. B. M. Allen *et al.*, Systemic dysfunction and plasticity of the immune macroenvironment in cancer models. *Nat. Med.* **26**, 1125–1134 (2020).
35. J. R. Palmeri *et al.*, Tregs constrain CD8+ T cell priming required for curative intratumorally anchored anti-4-1BB immunotherapy. Biorxiv[Preprint] (2023). 10.1101/2023.01.30.526116 (Accessed 2 February 2023).
36. J. M. Kim, J. P. Rasmussen, A. Y. Rudensky, Regulatory T cells prevent catastrophic autoimmunity throughout the lifespan of mice. *Nat. Immunol.* **8**, 191–197 (2007).
37. K. Lahl *et al.*, Selective depletion of $Foxp3^+$ regulatory T cells induces a scurfy-like disease. *J. Exp. Med.* **204**, 57–63 (2007).
38. J. Kim *et al.*, Cutting edge: Depletion of $Foxp3^+$ cells leads to induction of autoimmunity by specific ablation of regulatory T cells in genetically targeted mice. *J. Immunol.* **183**, 7631–7634 (2009).
39. S. A. Fisher *et al.*, Transient treg depletion enhances therapeutic anti-cancer vaccination. *Immun. Inflamm. Dis.* **5**, 16–28 (2017).
40. X. Li, E. Kostareli, J. Suffner, N. Garbi, G. J. Hämmerling, Efficient treg depletion induces T-cell infiltration and rejection of large tumors. *Eur. J. Immunol.* **40**, 3325–3335 (2010).
41. C. T. Mayer *et al.*, Few $Foxp3^+$ regulatory T cells are sufficient to protect adult mice from lethal autoimmunity. *Eur. J. Immunol.* **44**, 2990–3002 (2014).
42. F. S. Hodi *et al.*, Improved survival with ipilimumab in patients with metastatic melanoma. *New Engl. J. Med.* **363**, 711–723 (2010).
43. G. K. Abou-Alfa *et al.*, Tremelimumab plus durvalumab in unresectable hepatocellular carcinoma. *Nejm. Evid.* **1**, 54–63 (2022).
44. X. Du *et al.*, A reappraisal of CTLA-4 checkpoint blockade in cancer immunotherapy. *Cell Res.* **28**, 416–432 (2018).
45. A. Sharma *et al.*, Anti-CTLA-4 immunotherapy does not deplete $FOXP3^+$ regulatory T cells (Tregs) in human cancers. *Clin. Cancer Res.* **25**, 1233–1238 (2018).

46. A. Sharma *et al.*, Anti–CTLA-4 immunotherapy does not deplete FOXP3$^+$ regulatory T cells (Tregs) in human cancers-response. *Clin. Cancer Res.* **25**, 3469–3470 (2019).
47. R. Ferrara, S. Susini, A. Marabelle, Anti-CTLA-4 immunotherapy does not deplete Foxp3$^+$ regulatory T cells (Tregs) in human cancers-letter. *Clin. Cancer Res.* **25**, 3468 (2018).
48. D. Bauché *et al.*, Antitumor efficacy of combined CTLA4/PD-1 blockade without intestinal inflammation is achieved by elimination of FcγR interactions. *J. Immunother. Cancer* **8**, e001584 (2020).
49. M. Semmrich *et al.*, Vectorized Treg-depleting αCTLA-4 elicits antigen cross-presentation and CD8$^+$ T cell immunity to reject 'cold' tumors. *J. Immunother. Cancer* **10**, e003488 (2022).
50. K. M. van Pul *et al.*, Local delivery of low-dose anti–CTLA-4 to the melanoma lymphatic basin leads to systemic treg reduction and effector T cell activation. *Sci. Immunol.* **7**, eabn8097 (2022).
51. C. Williams *et al.*, Impact of CTLA-4 checkpoint antibodies on ligand binding and transendocytosis. *Front. Immunol.* **13**, 871802 (2022).
52. I. Yofe *et al.*, Anti-CTLA-4 antibodies drive myeloid activation and reprogram the tumor microenvironment through FcγR engagement and type I interferon signaling. *Nat. Cancer* **3**, 1336–1350 (2022).
53. J. D. Waight *et al.*, Selective FcγR Co-engagement on APCs modulates the activity of therapeutic antibodies targeting T cell antigens. *Cancer Cell* **33**, 1033–1047.e5 (2018).
54. D. R. Leach, M. F. Krummel, J. P. Allison, Enhancement of antitumor immunity by CTLA-4 blockade. *Science* **271**, 1734–1736 (1996).
55. E. M. Sotomayor, I. Borrello, E. Tubb, J. P. Allison, H. I. Levitsky, In vivo blockade of CTLA-4 enhances the priming of responsive T cells but fails to prevent the induction of tumor antigen-specific tolerance. *Proc. Natl. Acad. Sci. U.S.A.* **96**, 11476–11481 (1999).
56. P. D. Gregor *et al.*, CTLA-4 blockade in combination with xenogeneic DNA vaccines enhances T-cell responses, tumor immunity and autoimmunity to self antigens in animal and cellular model systems. *Vaccine* **22**, 1700–1708 (2004).
57. S. Demaria *et al.*, Immune-mediated inhibition of metastases after treatment with local radiation and CTLA-4 blockade in a mouse model of breast cancer. *Clin Cancer Res.* **11**, 728–734 (2005).
58. J. Hernández, A. Ko, L. A. Sherman, CTLA-4 blockade enhances the CTL responses to the p53 self-tumor antigen. *J. Immunol.* **166**, 3908–3914 (2001).
59. Y. Sato *et al.*, Fc-independent functions of anti-CTLA-4 antibodies contribute to anti-tumor efficacy. *Cancer Immunol. Immunother.* **71**, 2421–2431 (2022).
60. M. A. Curran, W. Montalvo, H. Yagita, J. P. Allison, PD-1 and CTLA-4 combination blockade expands infiltrating T cells and reduces regulatory T and myeloid cells within B16 melanoma tumors. *Proc. Natl. Acad. Sci. U.S.A.* **107**, 4275–4280 (2010).
61. S. A. Quezada, K. S. Peggs, M. A. Curran, J. P. Allison, CTLA4 blockade and GM-CSF combination immunotherapy alters the intratumor balance of effector and regulatory T cells. *J. Clin. Invest.* **116**, 1935–1945 (2006).
62. K. S. Peggs, S. A. Quezada, C. A. Chambers, A. J. Korman, J. P. Allison, Blockade of CTLA-4 on both effector and regulatory T cell compartments contributes to the antitumor activity of anti–CTLA-4 antibodies. *J. Exp. Med.* **206**, 1717–1725 (2009).
63. T. R. Simpson *et al.*, Fc-dependent depletion of tumor-infiltrating regulatory T cells co-defines the efficacy of anti–CTLA-4 therapy against melanoma. *J. Exp. Med.* **210**, 1695–1710 (2013).
64. M. J. Selby *et al.*, Anti-CTLA-4 antibodies of IgG2a isotype enhance antitumor activity through reduction of intratumoral regulatory T cells. *Cancer Immunol. Res.* **1**, 32–42 (2013).
65. Y. Bulliard *et al.*, Activating Fc γ receptors contribute to the antitumor activities of immunoregulatory receptor-targeting antibodies. *J. Exp. Med.* **210**, 1685–1693 (2013).
66. J. R. Ingram *et al.*, Anti–CTLA-4 therapy requires an Fc domain for efficacy. *Proc. Natl. Acad. Sci. U.S.A.* **115**, 3912–3917 (2018).
67. F. A. Vargas *et al.*, Fc effector function contributes to the activity of human anti-CTLA-4 antibodies. *Cancer Cell* **33**, 649–663 (2018).
68. D. Ha *et al.*, Differential control of human treg and effector T cells in tumor immunity by Fc-engineered anti–CTLA-4 antibody. *Proc. Natl. Acad. Sci. U.S.A.* **116**, 609–618 (2018).
69. M. Lo *et al.*, Effector-attenuating substitutions that maintain antibody stability and reduce toxicity in mice. *J. Biol. Chem.* **292**, 3900–3908 (2017).
70. E. L. Stone *et al.*, Lack of blocking activity in anti-CTLA-4 antibodies reduces toxicity, but not anti-tumor efficacy. BioRxiv[Preprint] (2021). https://doi.org/10.1101/2021.07.12.452090 (Accessed 14 July 2021).
71. R. L. Kelly, D. Le, J. Zhao, K. D. Wittrup, Reduction of nonspecificity motifs in synthetic antibody libraries. *J. Mol. Biol.* **430**, 119–130 (2018).
72. M. W. Traxlmayr *et al.*, Strong enrichment of aromatic residues in binding sites from a charge-neutralized hyperthermostable Sso7d scaffold library. *J. Biol. Chem.* **291**, 22496–22508 (2016).
73. A. W. Tisdale, *New Protein Engineering Approaches for Potentiating and Studying Antibody-Based EGFR Antagonism* (Massachusetts Institute of Technology, 2019).
74. B. H. Kang, B. M. Lax, K. D. Wittrup, Yeast surface display. *Methods Mol. Biol.* **2491**, 29–62 (2022).
75. J. B. Spangler *et al.*, Combination antibody treatment down-regulates epidermal growth factor receptor by inhibiting endosomal recycling. *Proc. Natl. Acad. Sci. U.S.A.* **107**, 13252–13257 (2010).
76. D. A. Ostrov, W. Shi, J.-C.D. Schwartz, S. C. Almo, S. G. Nathenson, Structure of murine CTLA-4 and its role in modulating T cell responsiveness. *Science* **290**, 816–819 (2000).
77. C. C. Stamper *et al.*, Crystal structure of the B7–1/CTLA-4 complex that inhibits human immune responses. *Nature* **410**, 608–611 (2001).
78. A. M. Rothschilds, *Engineering Protein-Based Modulators of Allergic, Temporal, and Checkpoint Blockade Anti-Cancer Immunity* (Massachusetts Institute of Technology, 2019).
79. N. Sharma, J. Vacher, J. P. Allison, TLR1/2 ligand enhances antitumor efficacy of CTLA-4 blockade by increasing intratumoral treg depletion. *Proc. Natl. Acad. Sci. U.S.A.* **116**, 10453–10462 (2019).
80. E. M. Schmidt *et al.*, CTLA-4 controls regulatory T cell peripheral homeostasis and is required for suppression of pancreatic islet autoimmunity. *J. Immunol.* **182**, 274–282 (2009).
81. F. A. Vargas *et al.*, Fc-optimized anti-CD25 depletes tumor-infiltrating regulatory T cells and synergizes with PD-1 blockade to eradicate established tumors. *Immunity* **46**, 577–586 (2017).
82. I. Solomon *et al.*, CD25-Treg-depleting antibodies preserving IL-2 signaling on effector T cells enhance effector activation and antitumor immunity. *Nat. Cancer* **1**, 1153–1166 (2020).
83. L. Deng *et al.*, Accumulation of Foxp3$^+$ T regulatory cells in draining lymph nodes correlates with disease progression and immune suppression in colorectal cancer patients. *Clin. Cancer Res.* **16**, 4105–4112 (2010).
84. Z. Li *et al.*, In vivo labeling reveals continuous trafficking of TCF-1$^+$ T cells between tumor and lymphoid tissue. *J. Exp. Med.* **219**, e20210749 (2022).
85. J. P. Hindley *et al.*, T-cell trafficking facilitated by high endothelial venules is required for tumor control after regulatory T-cell depletion. *Cancer Res.* **72**, 5473–5482 (2012).
86. E. J. Colbeck *et al.*, Treg depletion licenses T cell-driven HEV neogenesis and promotes tumor destruction. *Cancer Immunol. Res.* **5**, 1005–1015 (2017).
87. T. Fujita *et al.*, Inhibition of transforming growth factor-β–mediated immunosuppression in tumor-draining lymph nodes augments antitumor responses by various immunologic cell types. *Cancer Res.* **69**, 5142–5150 (2009).
88. A. Kennedy *et al.*, Differences in CD80 and CD86 transendocytosis reveal CD86 as a key target for CTLA-4 immune regulation. *Nat. Immunol.* **23**, 1365–1378 (2022).